

NUMERICAL SIMULATIONS OF THE CRITICAL DIAMETER AND FLAME STABILITY FOR HYDROGEN JET FLAMES

Kazemi, M.¹, Brennan, S.² and Molkov, V.³

¹ Hydrogen Safety Engineering and Research Centre (HySAFER) Centre, University of Ulster, Newtownabbey BT37 0QB, UK, Kazemi-m1@ulster.ac.uk

² sl.brennan@ulster.ac.uk

³ v.molkov@ulster.ac.uk

ABSTRACT

This study focuses on development of a CFD model able to simulate the experimentally observed critical nozzle diameter for hydrogen non-premixed flames. The critical diameter represents the minimum nozzle size through which a free jet flame will remain stable at all driving pressures. Hydrogen non-premixed flames will not blow-out at diameters equal to or greater than the critical diameter. Accurate simulation of this parameter is important for assessment of thermally activated pressure relief device (TPRD) performance during hydrogen blowdown from a storage tank. At TPRD diameters below the critical value there is potential for a hydrogen jet flame to blow-out as the storage tank vents, potentially leading to hydrogen accumulation in an indoor release scenario. Previous experimental studies have indicated that the critical diameter for hydrogen is approximately 1 mm. In this study flame stability is considered across a range of diameters and overpressures from 0.1 mm to 2 mm and from 0.2 MPa to 20 MPa, respectively. The impact of turbulent Schmidt number Sc_t , which is the ratio of momentum diffusivity (kinematic viscosity) and mass diffusivity, on the hydrogen concentration profile in the region near the nozzle exit, and subsequent influence on critical diameter was investigated and discussed. For lower Sc_t values, the enhanced mass mixing resulted in smaller predicted critical diameters. The use of value $Sc_t=0.61$ in the model demonstrated the best agreement with experimental values of the critical diameter. The model reproduced the critical diameter of 1 mm and then was applied to predict flame stability for under-expanded hydrogen jets.

NOMENCLATURE

C_p	constant pressure specific heat (J/kg/K)	Greek	
P	pressure (Pa)	ρ	density (kg/m ³)
U	velocity (m/s)	μ	dynamic viscosity (W/m ²)
T	temperature (K)	ν	kinematic viscosity (m ² /s)
E	total energy (J/kg)	ε	energy dissipation rate (m ² /s ²)
H	enthalpy (J/kg)	Subscripts	
g	gravity acceleration (m/s ²)	i, j, k	cartesian coordinate indexes
t	time (s)	m	chemical species
Sc	Schmidt number (-)	t	turbulent
Pr	Prandtl number (-)	E	energy
Y	mass fraction (-)	f	flame
D	molecular diffusivity (m ² /s),	s	surrounding
k	turbulent kinetic energy (m ² /s ²)	N	nozzle exit
τ	time scale of small-scale motions (s)	H_2	hydrogen
ξ	length scale of small-scale motions (-)	Superscripts	
G_k	the production of turbulence kinetic energy due to the mean velocity gradients (kg/m/s ³)	*	fine-scale quantities
G_b	the production of turbulence kinetic energy due to the buoyancy (kg/m/s ³)	Constants and model parameters	
S_{ij}	the mean rate-of-strain tensor (s ⁻¹)	$C_{1\varepsilon}$	1.44
S_E	energy source term (J/m ³ /s)	C_2	1.9
S_m	source term in chemical species transport (kg/m ³ /s)	σ_k	1.0
R		σ_ε	1.2

	net rate of production/destruction of species	C_τ	0.4082
r	(kg/m ³ /s)	C_ξ	2.137
	radius (m)		
L	length (m)		
d	diameter (m)		

1. INTRODUCTION

High-pressure gaseous hydrogen storage is the most common technology for onboard storage in automotive and rail applications as well as at stationary tanks at hydrogen refuelling stations. Where the tank or piping system is damaged, or the TPRD opens, the hydrogen released is likely to ignite resulting in an under-expanded jet fire. Depending on the stability of the flame, blow-out may occur, potentially leading to formation of a flammable cloud, especially for releases in confined spaces [1]. The ability to numerically predict blow-out phenomenon is important from a safety perspective.

1.1. Blow-out mechanism

The terms blow-off and blow-out have been used interchangeably in some studies, but Wu et al. [2] defined blow-out as extinguishment of a lifted flame and blow-off as extinguishment of an attached flame and this definition is used here. Different models have been proposed to explain flame stabilization. In 1965 Vanquickenborne and Van Tiggelen [3] suggested a premixed flame propagation model to predict lift-off height and structure of turbulent diffusion flames. The stabilization point of the flame was defined as a distance from the burner exit where turbulent burning velocity is equal to mean gas velocity, and blow-out occurs when the mean gas velocity exceeds the turbulent burning velocity. In 1984 Broadwell et al. [4] proposed another stabilization mechanism for turbulent diffusion flames, suggesting that large-scale turbulent eddies exiting from the nozzle expel hot gases to the lateral edge of the jet. Re-entrainment of the hot gases ignite the non-combusting turbulent structure in the jet. Flame stabilization occurs if the mixing time of the re-entrained hot gases is long enough, otherwise blow-out occurs. In 1996 Tieszen et al. [5] developed a correlation including the premixed flame mechanism and large-scale turbulent eddies. In 2006, Wu et al. [6] proposed blow-out occurs when the flame base is pushed downstream beyond the maximum waistline position and the flame becomes unstable.

1.2. Critical diameter

A key parameter for flame stability is critical diameter which represents the minimum nozzle size through which a free jet flame will remain stable at all driving pressures. When hydrogen is released through a nozzle where the diameter is equal or larger than the critical diameter, and it is ignited, the resultant flame is stable regardless of the reservoir pressure, which continuously reduces during emergency blowdown from a storage tank. In 1978 Annushkin and Sverdlov [7] estimated critical diameter for hydrogen as 1.01 mm. They propose a semi-empirical model to calculate lift-off and blow-out velocity, and consider the stability limit for propane, methane, and hydrogen non-premixed flames. In 1981 Kalghatgi [8] presented a correlation for the blow-out limit of sub-sonic jets, which was extrapolated for choked flows of fuels including hydrogen. He deduced there is a critical burner diameter above which the flame is stable regardless of gas flow rate. A value was not presented for hydrogen. In 1988, the critical diameter was experimentally determined for natural gas as roughly 30 mm by Birch et al. [9]. For nozzle diameters smaller than the critical value subsonic jet flames were unstable when flow velocity at the nozzle exit exceeded the blow-out velocity; flame re-stabilisation was confirmed at elevated driving pressures [9]. In 2002 Devaud et al. [1] performed numerical and experimental studies examining the stability of under-expanded H₂-CO flames and compared the results to the work of Kalghatgi et al. [8] and Birch et al. [9]. The critical diameter increased from 1 mm for pure hydrogen to 1.5 mm (at a pressure of 1.1 MPa) by adding 4% vol. of CO [1]. They concluded for their case that RANS was unable to properly capture the turbulent field in under-expanded flows.

1.3 Experimental studies of hydrogen flame stability

In 2009, conditions for a sustained hydrogen flame and blow-out limits were investigated by Mogi et al. [10] through a series of experiments with different nozzle diameters and release pressures. It is this seminal piece of work that is the basis for the numerical study presented here. The limits separating the zones of sustained flame and flame blow-out for hydrogen are given for low and high pressures limits. It was concluded that the lower pressure limit for blow-out was almost constant and independent of nozzle diameter, but the upper (“inverted”) limit of blow-out pressure reduced with increase of nozzle diameter. The critical diameter was estimated as 1 mm using the graph by Mogi et al. [10]; this was confirmed by the authors through personal communication. In 2018, the blow-out process of hydrogen under-expanded jet flames was studied by Yamamoto et al. [11]. They presented a flame stability limit curve based on reservoir pressure and nozzle diameter. While they did not use the term critical diameter, it was shown that the nozzle diameter through which the hydrogen jet flame was stable regardless of reservoir pressure was 1.12 mm. It was shown that for stable under-expanded flames, the flame base position is almost constant irrespective of nozzle diameter, but the maximum waistline position, where the radial distance of elliptic stoichiometric contour is a maximum, varies due to Mach disk diameter variation resulting from different reservoir pressures. Thus, the Mach disk variation stemming from the reservoir pressure change, gives rise to different maximum waistline positions. They concluded that, in line with the process proposed in 2006 by Wu et al. [6], by decreasing the reservoir pressure, the flame base height can exceed the maximum stoichiometric waistline position resulting in blow-out.

1.4 Numerical studies of hydrogen flame stability

The numerical study of hydrogen flame stability limits is challenging as it involves both subsonic and under-expanded hydrogen jets. The shock structure has been shown to affect flame stability phenomenon in under-expanded jets and thus cannot be neglected as discussed by Yamamoto et al. [11] and Takeno et al. [12]. The complexity of the underlying physical phenomena is not yet fully understood. In 2016, numerical simulations for prediction of hydrogen under-expanded flame lift-off and blow-out were performed by Shentsov et al. [13] using the renormalization group (RNG) k- ϵ turbulence model and eddy dissipation concept (EDC) model for turbulence-chemistry interaction. The results of three cases of 0.3, 0.4, 0.5 mm nozzle diameter and exit pressure of around 11 MPa were presented. Blow-out was observed for 0.3 mm and a stable lifted flame was obtained for 0.4 and 0.5 mm. These results are in line with the stability limits presented by Mogi et al. [10]. The effect of shock structure was not included in their study, as the real nozzle was replaced by a notional nozzle in simulations.

1.5 Turbulent Schmidt number

It has been shown that the flame stability behaviour observed in numerical experiments is strongly influenced by simulation parameters. The chemical kinetics model, turbulence-chemistry interaction, and turbulent model constants can all impact ignition characteristics and flame stability behaviour. In 2006 Keistler et al. [14] developed a novel numerical model based on the k- ω turbulent model accounting for variability of Sc_t and Prandtl numbers by adding equations of mass fraction and enthalpy variances and their dissipation rate in order to simulate supersonic hydrogen combustion in a scramjet. The results of the method closely matched experimental results of temperature distribution, prediction of recirculation zones around hydrogen injection location, ignition time, and ignition location. In 2012 Xiao et al. [15] followed the same approach as Keistler et al. [14] and showed that for a scheme of variable Sc_t , values of Sc_t can be as low as 0.16 at boundary regions or in mixing layers. In 2007 Ingenito et al. [16] states that species fluctuation must be considered in combustion modelling and proposed a constant Sc_t is not valid in supersonic regimes since it does not reproduce turbulent mixing correctly. They simulated a steady flame with $Sc_t=0.4$ and 0.6, in contrast, $Sc_t=0.7$ caused flame oscillation [16]. In the next year 2008 Ingenito et al. [17] developed a novel model for supersonic hydrogen combustion in a scramjet by introducing a transport equation for contribution of sub-grid scale kinetic energy and accounted for the effect of species fluctuations on turbulent diffusivity in fine turbulent structures. The model with Sc_t in the range 0.1-0.4 resulted in more stable flames compared to constant $Sc_t=0.7$ [17].

2. PROBLEM DESCRIPTION

The focus of this study is to validate a numerical model which predicts the critical diameter for hydrogen flames. This model can be used to build the hydrogen flame stability curve for a range of pressures and diameters. Although previous authors [1] were unable to capture the turbulent field in under-expanded flows with RANS, it has been shown here to capture the turbulent field and lift-off and blow-out behaviour. The computational cost was significantly lower compared to our previous LES study [18]. The experimental data of Mogi et al. [10], specifically the critical diameter based on the flame stability graph, was used to validate the model. Dispersion, and ignition of a constant pressure hydrogen release of 0.2 MPa through round nozzles with diameters from 0.8 mm to 2 mm were simulated to investigate critical diameter. A wider range of pressures and diameters were considered to understand flame stability. The releases and geometry (Section 4) were chosen to allow comparison with experimental data. Pressure losses in the piping were not accounted for here. In the experiments, compressed hydrogen gas was ejected horizontally through a circular nozzle. A pilot burner was used to ignite the hydrogen then turned off. Burner location and duration were not given [10]. A pressure transducer on the header measured gauge release pressure (different from stagnant storage pressure).

3. MODEL AND NUMERICAL APPROACH

ANSYS Fluent version 20.2 was used as a computational engine to solve the governing equations. A pressure-based solver was used, and the ideal gas law was applied to capture compressibility. The pressure range in this study was lower than 20 MPa and thus real gas effects are deemed negligible. However, several real gas simulations were run to confirm the ideal gas law was an appropriate assumption here. The SIMPLE method was used for pressure-velocity coupling. A second-order upwind scheme was used to discretise density, momentum, energy, and species transport equations. A first-order implicit scheme was used for temporal discretisation. A second-order scheme was used to interpolate pressure values at cell faces. The mass, momentum, energy, and species transport equations solved are:

$$\frac{\partial \rho}{\partial t} + \frac{\partial \rho U_i}{\partial x_i} = 0, \quad (1)$$

$$\frac{\partial(\rho U_i)}{\partial t} + \frac{\partial(\rho U_i U_j)}{\partial x_j} = -\frac{\partial p}{\partial x_i} + \frac{\partial}{\partial x_j} (\mu + \mu_t) \left(\frac{\partial U_i}{\partial x_j} + \frac{\partial U_j}{\partial x_i} - \frac{2}{3} \frac{\partial U_k}{\partial x_k} \delta_{ij} \right) + \rho g_i, \quad (2)$$

$$\frac{\partial(\rho E)}{\partial t} + \frac{\partial}{\partial x_i} (U_i(\rho E + p)) = \frac{\partial}{\partial x_i} \left[\left(k + \frac{\mu_t c_p}{Pr_t} \right) \frac{\partial T}{\partial x_i} - \sum_m h_m \left(-(\rho D_m + \frac{\mu_t}{Sc_t}) \right) \right] + \quad (3)$$

$$U_i (\mu + \mu_t) \left(\frac{\partial U_i}{\partial x_j} + \frac{\partial U_j}{\partial x_i} - \frac{2}{3} \frac{\partial U_k}{\partial x_k} \delta_{ij} \right) \Big] + S_E, \quad (4)$$

$$\frac{\partial(\rho Y_m)}{\partial t} + \frac{\partial}{\partial x_i} (\rho U_i Y_m) = \frac{\partial}{\partial x_i} \left[(\rho D_m + \frac{\mu_t}{Sc_t}) \frac{\partial Y_m}{\partial x_i} \right] + S_m, \quad (4)$$

The Kronecker symbol is defined as:

$$\delta_{ij} = \begin{cases} 1 & i = j \\ 0 & i \neq j \end{cases}. \quad (5)$$

3.1 Turbulence and combustion simulation approach

The realizable k- ϵ turbulence model [19] which is capable of predicting the spreading rate of axisymmetric jets [10] and was applied for simulations of hydrogen under-expanded jet fire by Cirrone et al. [21] was used to solve the turbulent kinetic energy (k) and dissipation rate equations (ϵ):

$$\frac{\partial(\rho k)}{\partial t} + \frac{\partial}{\partial x_i} (\rho k U_i) = \frac{\partial}{\partial x_i} \left[\left(\mu + \frac{\mu_t}{\sigma_k} \right) \frac{\partial k}{\partial x_i} \right] + G_k + G_b + \rho \epsilon + Y_m, \quad (6)$$

$$\frac{\partial(\rho \epsilon)}{\partial t} + \frac{\partial}{\partial x_i} (\rho \epsilon U_i) = \frac{\partial}{\partial x_i} \left[\left(\mu + \frac{\mu_t}{\sigma_\epsilon} \right) \frac{\partial \epsilon}{\partial x_i} \right] + \rho C_1 S_{ij} \epsilon - \rho C_2 \frac{\epsilon^2}{k + \sqrt{v \epsilon}} - C_{1\epsilon} \frac{\epsilon}{k} C_{3\epsilon} G_b, \quad (7)$$

where G_k and G_b represent the production of turbulence kinetic energy stemming from mean velocity gradients and buoyancy respectively. Y_m is the contribution of the effects of the fluctuating dilatation dissipation in compressible turbulent flows. σ_k and σ_ε represent turbulent Prandtl numbers for k and ε , corresponding to 1 and 1.2 respectively. $C_{3\varepsilon}$ is calculated as a function of the flow velocity components with respect to the gravitational vector. C_1 is evaluated as a function of the turbulent kinetic energy (k), dissipation rate equations (ε) and the modulus of the mean rate-of-strain tensor, S_{ij} . The EDC model was applied to simulate combustion. EDC is an extension of the eddy dissipation model [22]. One chemical reaction with 4 species was used for the reaction of hydrogen with air, thus water is the only product of the combustion. The source term in equation (4) is the net rate of production of species by chemical reactions defined as [23]:

$$R_m = \frac{\rho(\xi^*)^2}{\tau^*[1-(\xi^*)^3]} (Y_m^* - Y_m). \quad (8)$$

Time and length scale of small-scale motions are calculated as per Eqs. (9) and (10) [24]. C_τ and C_ξ are time scale and volume fraction constants of 0.4082 and 2.137 [24], R_m is the net rate of production/ destruction of species m by chemical reaction, Y_m is species m mass fraction in the surrounding fine-scales state, and Y_m^* is fine-scale mass fraction of species m after reacting over time τ^* :

$$\tau^* = C_\tau \left(\frac{v}{\varepsilon} \right)^{1/2}, \quad (9)$$

$$\xi^* = C_\xi \left(\frac{v\varepsilon}{k^2} \right)^{1/4}. \quad (10)$$

4. NUMERICAL DETAILS

4.1 Computational domain and mesh

The geometry and nozzle dimensions are shown in Figure 1. They replicate the experimental apparatus apart from two conical conjunction parts which were not detailed [10]. A cylindrical computational domain with a diameter of 6 m and a length of 13 m was considered large enough to eliminate the effect of boundaries on the flame and be applicable to a real scenario.

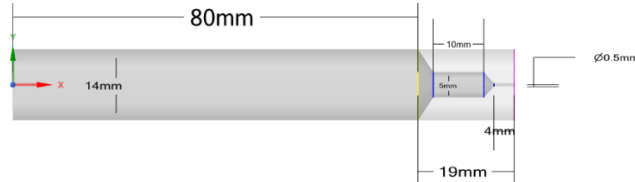


Figure 1. Nozzle geometry

Four hexahedral grids were considered for grid independence: “coarse”, “medium”, “fine #1”, and “fine #2”. These comprised roughly 70k, 200k, 400k and 1.5M control volumes (CVs). The nozzle was resolved by 4, 13, 20 and 26 CVs along the diameter. Minimum CVs are in the nozzle and are 0.2 mm, 0.06 mm, 0.04 mm and 0.03 mm. Minimum CV size for each grid was calculated for the smallest nozzle diameter (0.8 mm). Adequate resolution in the nozzle and vicinity is necessary to resolve the shock structure which was captured in all simulations. The example of “fine #1” grid is shown in Fig. 2.

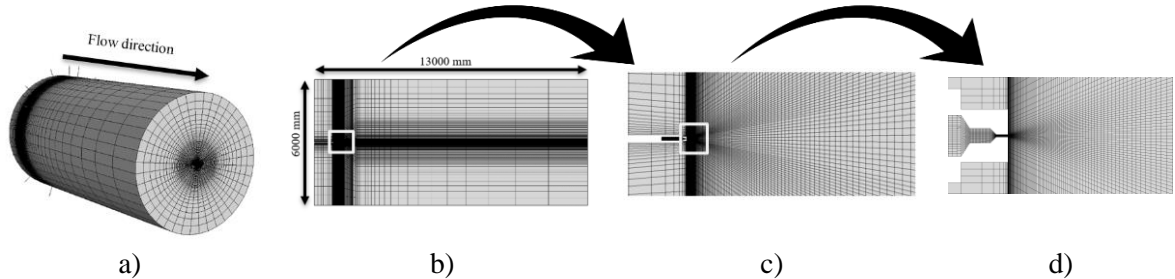


Figure 2. Grid “fine #1”: a) 3D computational domain; b) 2D centreline cross-section; c) zoomed-in view of cross-section near the lift-off distance; d) zoomed-in view of cross-section near the nozzle.

4.2 Boundary and initial conditions

The hydrogen inlet boundary condition was a pressure inlet located 98 mm from the nozzle exit where the pressure transducer in the experiments was mounted. A pressure outlet condition was applied for the radial and downstream boundary of the domain. A pressure inlet condition was applied for the upstream domain boundary. Non-reflecting boundary conditions were imposed at the boundaries (inlet and outlet). Hydrogen temperature and mass fraction were 300 K and 1 respectively at the hydrogen inlet boundary. Temperature, absolute pressure, and oxygen mass fraction were 300 K, 0.1 MPa, and 0.23, respectively. A no-slip condition was employed for all solid wall boundaries. To decrease computational cost, a steady-state solution of the unignited release was first simulated. Once the unignited jet had been established, the transient solution and combustion model was activated. The turbulence model and constants were the same for steady state and unsteady solutions. The pressure-based steady-state solver, the realizable k - ϵ turbulence model and coupled scheme were used in this initial unignited release stage.

4.3 Ignition simulation

To ignite the hydrogen-air mixture, a static temperature of 2400 K was patched in a cube region with dimensions of, e.g., x : 20-40 mm, y : 0-10 mm, and z : 5-10 mm. The ignition source was offset from the central axis of the domain so that flame formation and propagation of the flame back towards the nozzle could be clearly seen. Location of the pilot burner is not given in the experimental study. Care was taken to ensure the ignition source was appropriately located to ensure ignition would occur. Considering hydrogen concentration between the flammability limits and ensuring that the ignition source position does not affect flame extinguishment, the ignition source was located between the maximum stoichiometric waistline position and the nozzle exit. If a flame forms, its base should locate in this region [12]. According to experimental studies, if the ignition source were to be located where hydrogen concentration is less than 11%, the flame may be unstable and propagate downstream when the ignition source is present, or quench when the ignition source is removed [25]. Thus, the position of the numerical ignition source was determined based on the maximum waistline of the stoichiometric hydrogen concentration where it was 29.5% by volume in air, this differed for each diameter and pressure scenario. Water concentration was checked before deactivating the ignition source to ensure the mixture had ignited. Flame behaviour was investigated following removal of the ignition source.

5. RESULTS AND DISCUSSION

5.1 Grid and time step independence study

A mesh sensitivity study was performed in accordance with the CFD model evaluation protocol [26]. This study is focused on accurate prediction of the critical diameter, which in turn is influenced by both the hydrogen and velocity profiles in the jet prior to ignition. This is further discussed in terms of Sc_i in Section 5.3. Thus, two of the parameters investigated when considering grid independence were the hydrogen concentration and the velocity along the jet for the cold flow scenarios prior to ignition. Four grids were compared as noted in Section 4.1. Each grid refinement was defined with respect to the areas of interest including the zone close to nozzle exit where shock structure was captured, and flame anchoring occurred (lift-off distance). As described in Section 1.3 if the flame is stable, the flame base position will be located between the maximum waistline point and nozzle exit [5, 11]. Therefore, the number of cells along the nozzle diameter was increased in each stage of refinement and the mesh size was kept almost constant up to the maximum waistline point for each grid where the flame would be anchored. Hydrogen concentration and velocity decay along the central axis obtained from simulation for each grid system were compared and are presented in Fig. 3 and Fig. 4, for a release from a 1 mm nozzle diameter at 0.2 MPa pressure. Predicted concentration decay, based on the similarity law for hydrogen is included as a means of verification for behaviour downstream in the jet. The similarity law introduced by Chen and Rodi [27] was expanded and validated for hydrogen expanded and under-

expanded jets by Molkov [28]. Predictions using the velocity decay law, also validated for under-expanded jets by Molkov [28] are shown too. It should be emphasized that neither the velocity decay law, nor the similarity law are applicable for predictions near the nozzle. The concentration and velocity decay are:

$$Y_{H_2} = 5.4 \sqrt{\frac{\rho_N d}{\rho_S x}}, \quad (11)$$

$$\frac{U}{U_N} = 6.3 \sqrt{\frac{\rho_N d}{\rho_S x}}, \quad (12)$$

where ρ_N is hydrogen density at the nozzle exit [29] obtained for a release from a 1 mm nozzle diameter at 0.2 MPa, $\rho_S = 1.20 \text{ kg/m}^3$ is air density, and V_N is nozzle velocity [29] obtained for the same scenario.

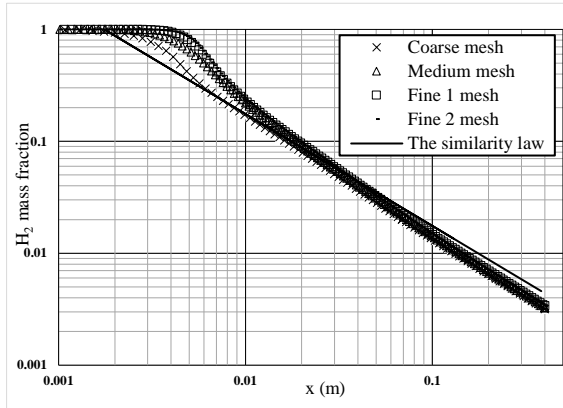


Figure 3. Hydrogen mass fraction axial decay for four meshes (release from 0.2 MPa through a 1 mm diameter nozzle).

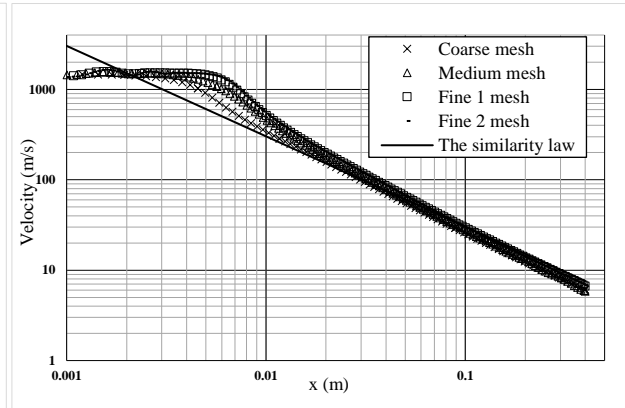


Figure 4. Hydrogen velocity axial decay for four meshes (release from 0.2 MPa through a 1 mm diameter nozzle).

As shown in Fig. 3 and Fig. 4 the results of “fine #1” grid and “fine #2” grids overlap, thus no further refinement was needed. Therefore, “fine #1”, the coarser of the two was selected for the study to reduce computational costs. Although “fine 1” grid was selected for the rest of the study, the critical diameter was obtained for the other grids to understand the degree of sensitivity of this parameter to grid resolution. It was confirmed that critical diameters of “course”, “medium”, “fine #1”, and “fine #2” were defined as 0.8, 0.9, 1, and 1 mm, respectively. For a coarser grid both the hydrogen and velocity were found to decay more quickly. Figures 3 and 4 show that hydrogen concentration decay is shorter, and velocity is lower in the coarse grid in the region close to the nozzle exit (distance from the nozzle exit to maximum waistline location along the axis is up to 35 mm). Thus, for a coarser grid a lower value of 0.8 mm was defined as the critical diameter in simulations. The predicted critical diameter increased with grid refinement to 1 mm until no difference was observed between “fine #1” and “fine #2” grids.

An implicit solution scheme was used, and a time-step size independence study was conducted to investigate the accuracy and stability of results. The cold flow simulations were steady state; thus, the time-step independence study was performed for the unsteady ignited stage where a quasi-steady solution had been reached. Temperature as a function of dimensionless axial distance (x/L_f) for a release through a 1 mm nozzle diameter from 0.2 MPa, for four different time-step sizes is shown in Figure 5. Experimental data for hydrogen flames [28] are included as a means of verification.

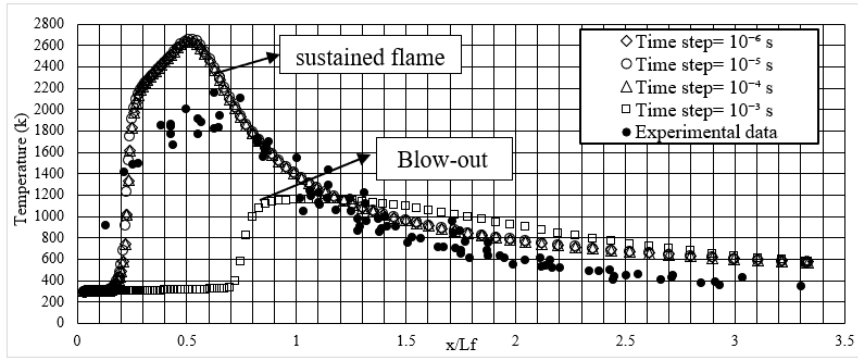


Figure 5. The temperature along the axis as a function of dimensionless distance by flame length

Temperature along the axis is the same for time steps of 10^{-4} , 10^{-5} , and 10^{-6} s. The results are clearly different for a time step of 10^{-3} s, where the flame became unstable and was found to numerically blow-out, indicating a simulated critical diameter larger than 1 mm. Temperatures for the scenario with a time step of 10^{-3} s dropped below 1300 K, considered as a flame visibility limit and hot products were to move downstream, exiting the domain. All scenarios were simulated for a flow time of 400 ms. Thus, 10^{-4} s was selected as the most appropriate time step to reduce the computational cost whilst reproducing the correct critical diameter. The adiabatic flame temperature of hydrogen is about 2400 K and higher values are evident in Fig. 5. Possible reasons are the application of a single step reaction mechanism for hydrogen combustion, neglecting the effect of flame radiation, zero response time of “numerical thermocouple”, pre-heating of fresh mixture due to the numerical requirement of 3-5 cells to simulate physical discontinuity, etc. The Discrete Ordinates radiation model was investigated. It was found to reduce the flame temperature by approximately 50 K and did not have any effect on flame blow-out or lift-off. Thus, it was not included in order to decrease computational costs.

5.2 Blow-out and sustained flames

To demonstrate what was considered as blow-out and a sustained flame in simulations, a comparison of what was observed numerically is presented. The same behaviour was observed in all blow-out cases, which was unlike the behaviour observed for sustained flames. A comparison of a lifted flame and blow-out scenarios based on temperature and water vapour concentration fields is shown in Fig. 6.

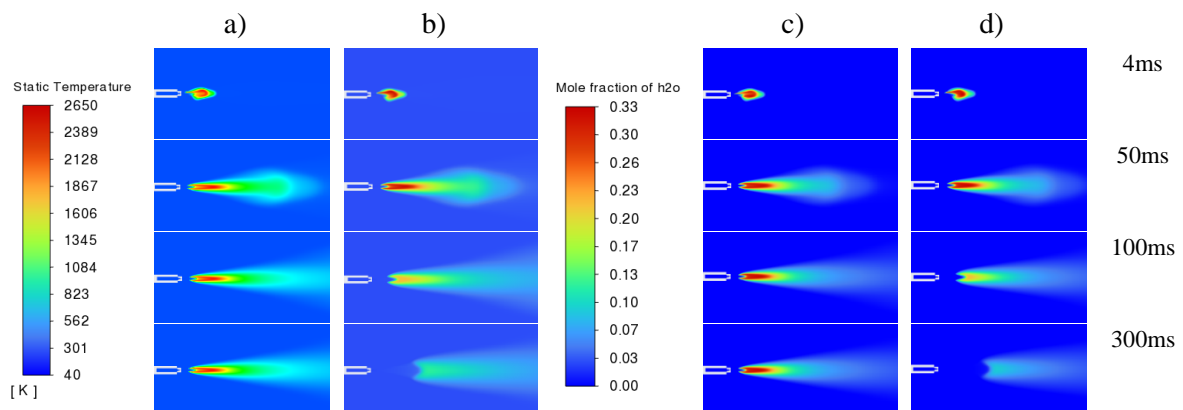


Figure 6. Sustained flame versus blow-out (0.2 MPa): a) Temperature (1 mm nozzle); b) Temperature (0.9 mm nozzle); c) Water mole fraction (1 mm nozzle); d) Water mole fraction (0.9 mm nozzle).

Note: a cropped domain is shown

The ignition source was applied until the flame can be seen to propagate around the axis and back towards the nozzle. On removal of the ignition source, in the blow-out scenario, a flame was formed, but it moved downstream of the domain and its temperature constantly diminished. In Fig. 6d, the same

behaviour could be seen in this scenario for water vapour as the combustion hot product propagating towards the domain exit. Blow-out is shown in Fig. 6b and Fig. 6d for a release pressure of 0.2 MPa and a 0.9 mm diameter nozzle. In the sustained flame scenario, the combustion region can be seen to expand and a sustained flame is established which remains unchanged after formation, see Fig. 6a. The hot products of combustion, water vapor, confirms the occurrence of sustained flaming as shown in Fig. 6c.

5.3 Effect of turbulent Sc number on the critical diameter

In accordance with definitions of blow-out phenomenon given by Vanquickenborne and Van Tiggelen [3], if the turbulent flame velocity becomes lower than the mean velocity of the flow, flame extinction will finally occur. In 1985 Byggstøy and Magnussen [30] presented a solution to the fuel concentration transport equation, then following simplifying the solution using k-ε model, they indicated that the turbulent flame propagation velocity is inversely proportional to Sc_t . To be more specific, by decreasing Sc_t , the turbulent flame velocity will increase. In this case, the mean flow velocity outweighs the turbulent burning velocity and, finally, leads to flame extinction or blow-out. In the present study, different Sc_t numbers, close to the generally accepted constant value of 0.7, were applied in simulations to investigate under which Sc_t number the critical diameter, where sustained flame exists unconditionally for all operating release pressures, fits well the experimental critical diameter of 1 mm measured experimentally [10, 11]. As shown in [Table 1](#), the best agreement was achieved for $Sc_t=0.61$. To determine the critical diameter, a series of simulations for varying nozzle diameter and a release pressure of 0.2 MPa were performed. Starting at 0.8 mm the nozzle diameter was increased in steps of 0.1 mm, until a sustained flame was observed. Additional simulations were performed as trials above and below release pressure of 0.2 MPa and resulted in sustained flame at the critical nozzle diameter. The same procedure was followed for $Sc_t=0.7$ and $Sc_t=0.6$ and results are shown in [Table 1](#).

Table 1. Critical diameter for different turbulent Schmidt number compared to experimental value.

	$Sc_t = 0.7$	$Sc_t = 0.61$	$Sc_t = 0.6$	Experiment
Critical diameter	2 mm	1mm	0.9mm	1mm

As described in Section 5.1, the hydrogen concentration profile in the near nozzle region strongly influences flame stability. By changing Sc_t hydrogen concentration is impacted. For lower Sc_t species mixing is enhanced, and smaller critical diameters are predicted. When concentration profiles for small changes in Sc_t are compared the difference is very small. Hence results of releases with $Sc_t=0.3$ and $Sc_t=1.1$ are included here as the difference is more pronounced. Hydrogen concentration field is shown in Fig. 7 for cold flow release from 0.2 MPa through a 1 mm nozzle with $Sc_t=0.3$ and $Sc_t=1.1$. The jet with the lower Sc_t has a wider expansion angle. This wider expansion, stemming from the lower Sc_t , leads to greater maximum distance in radial direction perpendicular to nozzle axis on the elliptic stoichiometric contour where the flame tip would be anchored (see Fig. 8), subsequently, as shown in Fig. 9 the flow velocity at this point is almost half the velocity as in the scenario with $Sc_t = 1.1$.

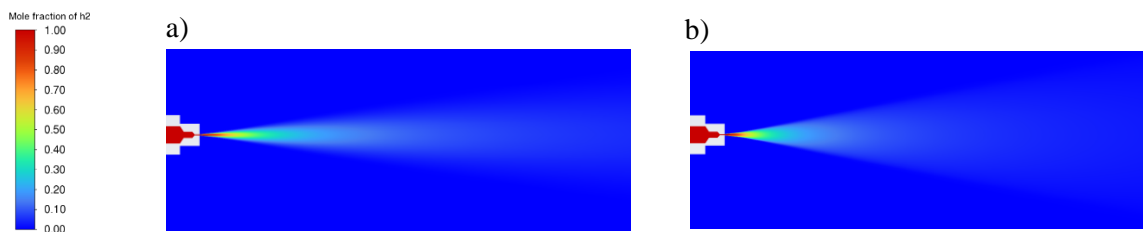


Figure 7. Hydrogen mole fraction for cold flow (release from 0.2 MPa through a 1 mm nozzle diameter): a) $Sc_t=1.1$ leading to blow-out; b) $Sc_t=0.3$ leading to sustained flame

As presented by Vanquickenborne and Van Tiggelen [3], lower flow velocity increases the chance of a sustained flame. In Fig. 8, 29.5% by volume demonstrates the stoichiometric hydrogen concentration.

The maximum waistline intersected the elliptic stoichiometric contour at radial positions of ± 3.8 mm and ± 4.7 mm for scenarios with $Sc_t=1.1$ and $Sc_t=0.3$. Cold flow velocity values corresponding to these radial positions are approximately 42 m/s and 22 m/s as indicated in Fig. 9. Results are shown for relatively low and high Sc_t numbers of 0.3 and 1.1, along with $Sc_t=0.6$ and $Sc_t=0.7$ as these are representative of those used in this study. Although the difference for $Sc_t=0.6$ and $Sc_t=0.7$ is small, it is sufficient to influence the prediction of critical diameter. The flow velocity for $Sc_t=0.3$ is smaller, but the turbulent burning velocity is higher than the case with $Sc_t=1.1$, as noted by Byggstøyl and Magnussen [30], these two factors lead to a sustained flame and blow-out for the scenarios with $Sc_t=0.3$ and $Sc_t=1.1$, respectively. Thus, there is a Sc_t number by which the hydrogen concentration would be reproduced accurately leading to prediction of the correct critical diameter as determined by the experiments. Sc_t represents the ratio between turbulent momentum diffusivity, ν_t , and turbulent mass diffusivity, D_t . For lower Sc_t values turbulent mass transport becomes more significant and outweighs the turbulent momentum diffusion, meaning fuel-air mixing is enhanced, increasing the possibility of a sustained flame. Improvement in turbulent mass diffusion, particularly in the mixing layer, where hydrogen meets quiescent surrounding air means the angle of the hydrogen jet spread is augmented. Whilst the focus of this work is on the near nozzle behaviour, and the critical diameter, wider verification of the jet parameters was considered. To verify jet shape, the jet angle was measured and compared with the turbulent free jet angle calculated by Tollmien reported to be 12° for the half-angle [31]. Although the concentration limit for assertion of hydrogen jet boundaries is not a certain value and the release pressure influences density which has effect on jet concentration, the estimated value provided by Tollmien [31] supports the accuracy of the jet profile simulated in this study. Considering 1% as the value of hydrogen mole fraction at the boundaries of a hydrogen jet, the jet half-angle was estimated as 12° , 11° , 13° , and 9° for Sc_t numbers of 0.6, 0.7, 0.3, and 1.1, respectively. Furthermore, there was no difference between jet half-angles for Sc_t numbers of 0.6 and 0.61. All the jet half-angles will be roughly 1 degree less if hydrogen mole fraction is equal to 4% at the boundaries of the hydrogen jet.

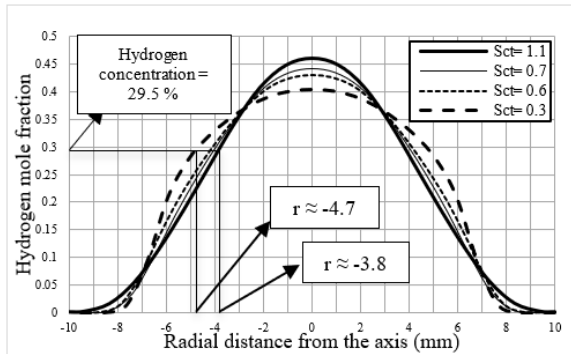


Figure 8. Hydrogen mole fraction as a function of radial distance at maximum waistline position for four different Sc_t numbers.

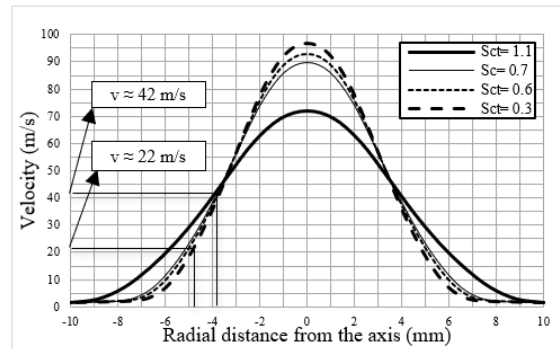


Figure 9. Velocity as a function of radial distance from the axis at maximum waistline position for four different Sc_t numbers

Flame length and width for the jet released through 1 mm nozzle at 0.2 MPa with $Sc_t=0.61$ was compared with experimental data. Using the novel dimensionless flame length correlation of Molkov [28] the flame length for a release through a 1 mm nozzle at 0.2 MPa pressure is predicted as 345 mm. The region between 1300 K and 1500 K was taken as the visible flame in simulations [32] where estimated values for flame length and width were 319 mm and 42 mm; a difference of 8% and 5%, respectively. It should be noted that the flame length and width were almost unaffected by Sc_t number for scenarios with sustained flames. Flame length and width for $Sc_t=0.3$ was less than 3% larger than with $Sc_t=0.61$.

5.4 Hydrogen flame stability limit

The model validated against the critical diameter was used to find two limiting points: release pressure of 0.6 MPa and 16 MPa through nozzle diameters of 0.1 and 0.3 mm, respectively, on the hydrogen flame stability curve [obtained](#) by Mogi et al. [10] enabling prediction of an approximate curve. Whilst the results shown below are for $Sc_t=0.61$, it should be noted that higher and lower Sc_t values were also

checked to ensure that the model validated for the critical diameter was applicable for different diameters and pressures, reflecting a wider range of conditions.

Table 2. Flame behaviour for simulated releases through 0.1 mm and 0.3 mm diameter nozzles.

Nozzle diameter (mm)	Release pressure (MPa)	Flame status
0.3	16	Blow-out
0.3	17	Blow-out
0.3	18	Blow-out
0.3	19	Blow-out
0.3	20	Sustained flame
0.1	0.6	Blow-out
0.1	0.5	Blow-out
0.1	0.4	Sustained flame

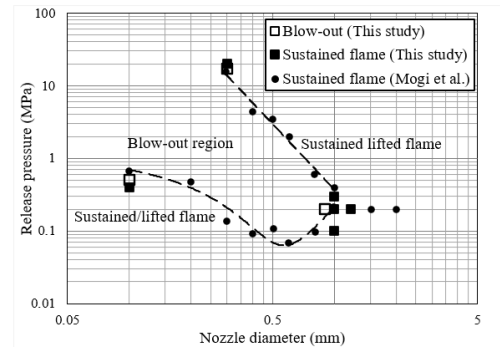


Figure 10. Hydrogen flame stability limit: experiments versus simulations ($Sc_t=0.61$)

The validated model can potentially be used to predict the whole curve, working with the hypothesis that if a model can reproduce the critical diameter consistent with experiments it will reproduce the stability curve; Figure 10 supports this as it shows the limiting points, predicted using the validated model. Although a limited number of points on the curve were included as this is beyond the scope of the paper, the trend agrees well with experiments. Two examples of simulations run to predict stability limits are given in Table 2. The points represent the stability limit in the upper and lower curves at positions furthest away from the critical diameter. For the lower limit and a 0.1 mm nozzle diameter, a release pressure starting from 0.6 MPa was decreased in steps of 0.1 MPa until a sustained flame was observed. For the upper limit, and a 0.3 mm nozzle diameter, the release pressure was increased from 16 MPa in steps of 1 MPa until a sustained flame was observed.

6. CONCLUSIONS

The *originality* of this work is the numerical prediction of the critical diameter for hydrogen and the insight given on the influence of model parameters on this. The validated modelling approach can be used to determine hydrogen flame stability for a range of pressures and diameters. Sustained flames, blow-out, and the limit at which the transition to or from blow-out occurs have been successfully simulated. Sc_t was shown to affect flame stability. A critical diameter of 1 mm which aligns to that obtained experimentally was predicted for $Sc_t=0.61$.

This study is *significant* for hydrogen safety engineers especially those using CFD models. Understanding of blow-out is important for piping and TPRD design. Where blow-out occurs in a confined space there is potential for hydrogen accumulation and formation of a flammable atmosphere. Flame stability should be accounted for in design, and the model described presents a means to do this.

The *rigour* of this work is in both the validation and verification of the model. The predicted critical diameter for hydrogen of 1 mm aligns to that determined in experiments. Results were shown to be grid independent and time step convergent. The model was applied to predict flame stability for diameters below the critical value.

REFERENCES

1. Devaud, C.B., Kelman, J.B., Moss, J.B. and Stewart, C.D., Stability of underexpanded supersonic jet flames burning H₂-CO mixtures, *Shock Waves*, **12**, No. 3, 2002, pp. 241–249.
2. Wu, Y., Al-Rahbi, I.S., Lu, Y. and Kalghatgi, G.T., The stability of turbulent hydrogen jet flames with carbon dioxide and propane addition, *Fuel*, **86**, No. 12-13, 2007, pp.1840-1848.

3. Vanquickenborne, L. and Van Tiggelen, A., The stabilization mechanism of lifted diffusion flames, *Combustion and Flame*, **10**, No. 1, 1966, pp. 59–69.
4. Broadwell, J.E., Dahm, W.J.A. and Mungal, M.G., Blowout of Turbulent Diffusion Flames, Proceedings of the Twentieth Symposium (International) on Combustion, 1984, pp. 303–310.
5. Tieszen, S.R., Stamps, D.W. and O’Hern, T.J., A heuristic model of turbulent mixing applied to blowout of turbulent jet diffusion flames, *Combustion and Flame*, **106**, No. 4, 1996, pp. 442–462.
6. Wu, C.Y., Chao, Y.C., Cheng, T.S., Li, Y.H., Lee, K.Y. and Yuan T., The blowout mechanism of turbulent jet diffusion flames, *Combustion and Flame*, **145**, No. 3, 2006, pp. 481–494.
7. Annushkin, Y.M. and Sverdlov, E.D., Stability of submerged diffusion flames in subsonic and underexpanded supersonic gas-fuel streams, *Comb., Expl. and Shock Waves*, **14**, 1978, pp. 597–605.
8. Kalghatgi, G.T., Blow-out stability of gaseous jet diffusion flames. Part I: in still air, *Combustion Science and Technology*, **26**, No. 5–6, 1981, pp. 233–239.
9. Birch, A.D., Brown, D.R., Cook, D.K. and Hargrave, G.K., Flame Stability in Underexpanded Natural Gas Jets, *Combustion Science and Technology*, **58**, No. 4–6, 1988, pp. 267–280.
10. Mogi, T. and Horiguchi, S., Experimental study on the hazards of high-pressure hydrogen jet diffusion flames, *Journal of Loss Prevention in the Process Industries*, **22**, No. 1, 2009, pp. 45–51.
11. Yamamoto, S., Sakatsume, R. and Takeno, K., Blow-off process of highly under-expanded hydrogen non-premixed jet flame, *Int. J. Hydrogen Energy*, **43**, No. 10, 2018, pp. 5199–5205.
12. Takeno, K., Yamamoto, S., Sakatsume, R., Hirakawa, S., Takeda, H., Shentsov, V., Makarov, D. and Molkov, V., Effect of shock structure on stabilization and blow-off of hydrogen jet flames, *Int. J. Hydrogen Energy*, **45**, No. 16, 2020, pp. 10145–10154.
13. Shentsov, V., Sakatsume, R., Makarov, D., Takeno, K. and Molkov, V., Lift-off and blow-out of under-expanded hydrogen jets: experiments versus simulations, Proceedings of the 8th International Seminar on Fire and Explosion Hazards (ISFEH8), 25-28 April 2016, University of Science and Technology of China.
14. Keistler, P.G., Xiaof, X., Hassan, H.A. and Rodriguez, C.G., Simulation of supersonic combustion using variable turbulent Prandtl/Schmidt number formulation, Collect. Tech. Pap. - 36th AIAA Fluid Dyn. Conf., 2006, pp. 2155–2167.
15. Xiao, X., Edwards, J.R., Hassan, H.A. and Cutler, A.D., Variable Turbulent Schmidt-Number Formulation for Scramjet Applications, *AIAA Journal*, **44**, No. 3, 2012, pp. 593–599.
16. Ingenito, A. and Bruno, C., Advance in LES modelling: Effect of the Turbulent Schmidt number on Supersonic Regime, 43rd AIAA/ASME/SAE/ASEE Joint Propulsion Conference & Exhibit, 2007, p. 5633.
17. Ingenito A. and Bruno C., Mixing and combustion in supersonic reactive flows, 44th AIAA/ASME/SAE/ASEE Joint Propulsion Conference & Exhibit, 2008, p. 4574.
18. Kazemi, M., Brennan, S. and Molkov, V., Numerical modelling of sustained hydrogen combustion and flame blow-off from a TPRD, Proceedings of the 10th International Seminar on Fire and Explosion Hazards (ISFEH10), 22-27 May 2022, Oslo.
19. Shih, T.H., Liou, W.W., Shabbir, A., Yang, Z. and Zhu, J., A new $k-\epsilon$ eddy viscosity model for high reynolds number turbulent flows, *Computers and Fluids*, **24**, No. 3, 1995, pp. 227–238.
20. ANSYS Fluent Theory Guide, Ansys Inc. Canonsburg, PA, USA, 2020.
21. Cirrone, D.M.C., Makarov, D., and Molkov, V., Simulation of thermal hazards from hydrogen under-expanded jet fire, *Int. J. Hydrogen Energy*, **44**, No. 17, 2019, pp. 8886–8892.
22. Magnussen, B.F., On the structure of turbulence and a generalized eddy dissipation concept for chemical reaction in turbulent flow, In 19th aerospace sciences meeting, 1981, p. 42.
23. Magnussen, B.F., Modeling of pollutant formation in gas turbine combustors based on the eddy dissipation concept, Eighteenth International Congress on Combustion Engines, Tianjin, China, 1989.
24. Gran, I.R. and Magnussen, B.F., A Numerical Study of a Bluff-Body Stabilized Diffusion Flame. Part 2. Influence of Combustion Modeling And Finite-Rate Chemistry, *Combust. Sci. Technol.*, **119**, No. 1–6, 1996, pp. 191–217.

25. Vesper, A., Kuznetsov, M., Fast, G., Friedrich, A., Kotchourko, N., Stern, G., Schwall, M. and Breitung, W., The structure and flame propagation regimes in turbulent hydrogen jets, *Int. J. Hydrogen Energy*, 36, No. 3, 2011, pp. 2351–2359.
26. Baraldi, D., Melideo, D., Kotchourko, A., Ren, K., Yanez, J., Jedicke, O., Giannissi, S.G., Toliás, I.C., Venetsanos, A.G., Keenan, J., Makarov, D., Molkov, V., Slater, S., Verbecke, F. and Duclos, A., Development of a model evaluation protocol for CFD analysis of hydrogen safety issues the SUSANA project, *Int. J. Hydrog. Energy*, 42, 2017.
27. Chen, C.J. and Rodi, W., Vertical turbulent buoyant jets: a review of experimental data, NASA Sti/Recon Tech. Rep. A, 80, 1980, p. 23073.
28. Molkov, V., Fundamentals of hydrogen safety engineering, 2012, www.bookboon.com.
29. Molkov, V. and Bragin, M., High-pressure hydrogen leak through a narrow channel, *Nonequilibrium Phenom. Plasma, Combust. Atmos.*, 2009, pp. 332–338.
30. Byggstoyl, S. and Magnussen, B.F., Model for flame extinction in turbulent flow., *Turbulent Shear Flows 4*, 1985, pp. 381–395.
31. Tollmien, W., Berechnung turbulenter ausbreitungsvorgänge, *ZAMM-Journal Appl. Math. Mech. für Angew. Math. und Mech.*, 6, No. 6, 1926, pp. 468–478.
32. Schefer, R., Houf, B., Bourne, B. and Colton, J., Experimental measurements to characterize the thermal and radiation properties of an open-flame hydrogen plume, In Proceedings of the 15th annual hydrogen conference and hydrogen expo, 2004.